Inorganic Chemistry

pubs.acs.org/IC

Article

High-Frequency and -Field Electron Paramagnetic Resonance Studies of Yellow/Orange/Red Pigments Based on Fe^{3+} in Trigonal Bipyramidal Coordination

J. Krzystek,* Joshua Telser, Peng Jiang, Gopika M. Gopakumar, and Mas A. Subramanian*

Cite This: https://doi.org/10.1021/acs.inorgchem.6c01324

Read Online

ACCESS | Metrics & More | Article Recommendations | Supporting Information

ABSTRACT: The material $YInO_3$ is amenable to doping of its trigonal bipyramidal (TBP) In^{3+} site by a wide range of metal ions. Among these are Mn^{3+} (S = 2) and Fe^{3+} (S = 5/2). The former, $YIn_{1-x}Mn_xO_3$, was previously the subject of an earlier investigation by high-frequency and -field electron paramagnetic resonance (HFEPR) spectroscopy. HFEPR is here applied to $YIn_{1-x}Fe_xO_3$ ($0 \le x \le 0.3$). This material exhibits a strong HFEPR response and spectra that can be readily analyzed using an S = 5/2 spin Hamiltonian with only second-order zero-field splitting (zfs) terms: $D = -1.095\ cm^{-1}$, E = 0. The spectral appearance is strongly dependent on both temperature and iron doping level, even for these In-rich samples. The zfs is semiquantitatively analyzed using a ligand-field theory (LFT) model, which suggests that the small-magnitude, negative D value arises from spin−orbit coupling (SOC) of the $^6A_1'$ (in D_{3h} idealized point group symmetry) ground state primarily with the lowest-lying $^4E''$ excited state.

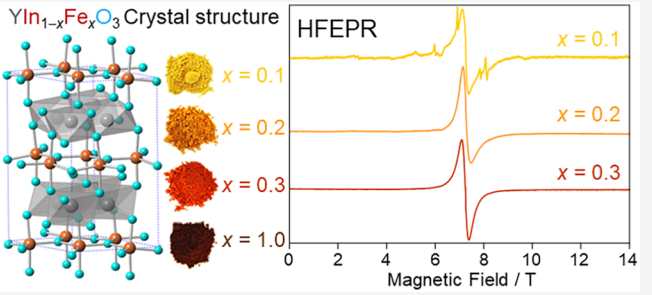

1. INTRODUCTION

The discovery of YInMn blue ($YIn_{1-x}Mn_xO_3$) with an intense blue color through Mn^{3+} substitution at trigonal bipyramidal (TBP) sites has led to a search for inorganic pigments with chromophore ions in TBP coordination.[1] Various colors from orange, to green, to purple are produced by introducing transition-metal cations Fe^{3+}, Cu^{2+}/Ti^{4+}, and $Mn^{3+}/Zn^{2+}/Ti^{4+}$ into the TBP In^{3+} sites in hexagonal $YInO_3$.[2−4] The origin of the resulting colors is presumably attributed to the crystal field splitting of the various paramagnetic ions associated with their TBP coordination and the short apical M−O bond distances (M = Fe^{3+}, Cu^{2+}, Mn^{3+}).

Hexagonal $YFeO_3$ is a metastable compound, which is normally prepared by a sol−gel method.[5,6] Hexagonal $YIn_{1-x}Fe_xO_3$ solid solutions however are prepared in two different ways depending on the Fe concentration.[2] The standard solid-state synthesis approach is successful for the preparation of In-rich phases from x = 0.0 to 0.3. The solution route has to be adopted for the preparation of Fe-rich phases from x = 0.7 to 1.0. A miscibility gap exists for the intermediate x ($0.3 < x < 0.7$) values. All $Y(In,Fe)O_3$ phases crystallize in a ferrielectric structure (space group $P6_3cm$) consisting of alternating layers of edge-shared YO_6 octahedra and corner-shared MO_5 (M = In, Fe) trigonal bipyramids along the c axis (Figure 1). While pure $YInO_3$ is off-white and $YFeO_3$ is reddish brown, the mixed system displays a color varying from yellow, to orange, to red brown due to the Fe^{3+}−O^{2-} charge transfer as well as the lower energy d−d transitions of Fe^{3+}.[7]

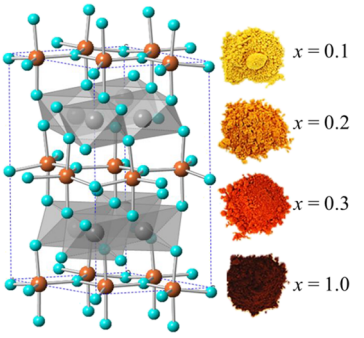

Figure 1. (left) Crystal structure of $YIn_{1-x}Fe_xO_3$ showing layers of MO_5 (M = In, Fe) trigonal bipyramids (TBP) interspersed with layers of YO_6 octahedra (Y, gray spheres; In/Fe, orange spheres; O, turquoise spheres). (Right) Colors of $YIn_{1-x}Fe_xO_3$ samples varying from yellow to orange and red brown with increasing Fe content (x = 0 is off-white).

Magnetometric measurements confirm high-spin (S = 5/2) Fe^{3+} for all phases.[2]

Received: March 12, 2026
Revised: May 4, 2026
Accepted: May 8, 2026

Importantly, understanding the electronic structure of transition-metal ions in oxide hosts is central to the rational design of new functional pigments. Such insight is particularly valuable for the development of environmentally benign, nontoxic inorganic pigments, especially yellow, orange, and red pigments that could serve as safer alternatives to conventional pigments containing hazardous elements such as Cd, Hg, and Pb.

The discovery of YInMn Blue and related pigments introduced a rare combination of intense color, chemical stability, and strong near-infrared reflectivity, meaning they reflect heat while remaining vividly colored. This makes them valuable for energy-efficient "cool" coatings on buildings and materials, helping reduce heat absorption and lower cooling costs. Additionally, they are nontoxic compared to many traditional pigments, making it safer for widespread commercial use.[7]

Although it is not as widely studied as its orthorhombic perovskite counterpart, hexagonal $YFeO_3$, along with its solid solutions, has been reported to show a variety of interesting structural, optical, catalytic, and dielectric properties.[2,6−10] The presence of paramagnetic Fe^{3+} ion also imparts distinct magnetic properties to the hexagonal $Y(In,Fe)O_3$ materials. Both neutron diffraction and magnetic susceptibility data suggest magnetic ordering of $YFeO_3$ at low temperatures.[2] Little has been reported however regarding the use of electron paramagnetic resonance (EPR) for such systems.

We have previously investigated the behavior of paramagnetic Mn^{3+} in hexagonal $Y(In,Mn)O_3$ by high-frequency and -field EPR (HFEPR).[11] The HFEPR technique is well suited to investigating metal ions with high-spin ground states, $S > 1/2$, particularly those with integer spin (non-Kramers ions), among which Mn^{3+} ($3d^4$, $S = 2$) has been especially fruitful.[12−24] HFEPR, however, can also be usefully applied to half-integer spin (Kramers ions), such as high-spin Co^{2+} ($3d^7$, $S = 3/2$).[25−27] High-spin Fe^{3+} ($3d^5$, $S = 5/2$) is another such Kramers ion, which, while readily observable using conventional EPR (typically X-band, $\nu \approx 9.5$ GHz),[28] can be studied more quantitatively using HFEPR as shown by Groenen and others.[29−32] In this work, we present an HFEPR study for the hexagonal $YIn_{1-x}Fe_xO_3$ ($x = 0.0−0.3$) solid solutions.

2. EXPERIMENTAL SECTION

Synthesis

A standard solid-state method was used to prepare the In-rich $YIn_{1-x}Fe_xO_3$ ($0 \le x \le 0.3$) phases. Stoichiometric amounts of Y_2O_3 (Research Chemicals, 99.99%), In_2O_3 (Alfa, 99.99%), and Fe_2O_3 (JMC, 99.999%) were mixed and ground in an agate mortar. The powder mixtures were pelletized and heated at 1200 °C for 12 h in air. The sintered pellets were then ground, pelletized, and heated again at 1300 °C for another 12 h. The phase purity of the samples was examined by X-ray powder diffraction (XRD). The XRD patterns were obtained at room temperature using a Rigaku MiniFlex diffractometer with Cu Kα radiation and a graphite monochromator.

HFEPR

HFEPR spectra were recorded using a spectrometer based on a 15/17 T superconducting magnet, differing from that previously described[33] only by the use of a Virginia Diodes Inc. (Charlottesville, Virginia, USA) source operating at a base frequency of 12−14 GHz and increased by a cascade of multipliers. The highest harmonic of the base frequency employed in the experiment was 24.

Spin Hamiltonian (SH)

The spectra and their frequency dependencies were simulated using software SPIN from Dr. A. Ozarowski (NHMFL) using the standard spin Hamiltonian:

$$H = \mu_B \boldsymbol{B}\cdot\boldsymbol{g}\cdot\hat{\boldsymbol{S}} + \hat{\boldsymbol{S}}\cdot\boldsymbol{D}\cdot\hat{\boldsymbol{S}}$$
$$= \mu_B \boldsymbol{B}\cdot\boldsymbol{g}\cdot\hat{\boldsymbol{S}} + D(\hat{S}_z^{\,2} - S(S+1)/3) + E(\hat{S}_x^{\,2} - \hat{S}_y^{\,2})$$

where μ_B is the Bohr magneton, $\mathbf{g}$ is the spectroscopic g-tensor, D and E are respectively the axial and rhombic second-order zero-field splitting (zfs) parameters. Although the spin Hamiltonian for an $S = 5/2$ system such as high-spin Fe^{3+} can include fourth-order zfs terms,[34] these were not needed to be invoked in the present case.

Ligand-Field Theory (LFT)

These calculations used the locally written program DDN and Ligfield software from Prof. J. Bendix (U. of Copenhagen, Denmark).[35] Both programs use the full d^5 basis set with angular overlap model (AOM) bonding parameters and interelectronic repulsion and SOC terms.

3. RESULTS

3.1. XRD and General HFEPR

All powder XRD patterns of the In-rich $Y(In,Fe)O_3$ samples show the superstructure peaks indicative of the ferrielectric structure shown in Figure 1. The $YIn_{1-x}Fe_xO_3$ ($0 \le x \le 0.3$) materials produced an excellent HFEPR response in any conditions, at any concentration of Fe^{3+}. There were basically three experimental variables in the experiments that could be followed: operating frequency, temperature, and Fe^{3+} concentration x (x = 0.1, 0.2, and 0.3). In the following, we will present the HFEPR results as a function of a single variable at a time.

3.2. Varying the HFEPR Operating Frequency, with Temperature and Concentration Constant

A typical HFEPR spectrum of $YIn_{0.9}Fe_{0.1}O_3$, i.e., at the lowest Fe^{3+} concentration, at 203.2 GHz and 10 K is shown in Figure 2. The spectrum can be immediately recognized as originating from a high-spin ($S = 5/2$) species, which is characteristic for Fe^{3+} in a nonheme (nonporphyrin) coordination (porphyrin-coordinated Fe^{3+} systems exhibit very different spectral signatures[36−38]). Indeed, the spectrum can be very satisfactorily simulated (the three, colored traces in Figure 2) assuming a powder distribution of the crystallites and a spin Hamiltonian with the following parameters: $|D| = 1.095$ cm^{-1}, $E = 0$, $g_\perp = 2.007$, $g_\parallel = 2.004$. Note that the parameters were obtained not from single-frequency spectra, but from a multifrequency data set by a simultaneous least-squares fit to all the turning points in the spectra collected at all the frequencies (Figure 3), the methodology called "tunable-frequency EPR".[39] Single-frequency simulations, on the other hand, were very useful in determining the sign of D: From the similarity of particular turning point intensities with simulations, it is apparent that D is negative.

Analogous spectra and simulations at a frequency lower and higher, respectively, than that at which the spectrum in Figure 2 was recorded are shown in Figures S1 and S2 in the Supporting Information (SI). What is quite striking is that some of the turning points at low temperature (10 K) consist of two components: a feature of relatively narrow width (a single-crystal line width used in the simulations was 25 mT) and another one of a broader width (the line width of 125 mT), independent of the operational frequency. The resonance fields at which these turning points appear are the same for the

https://doi.org/10.1021/acs.inorgchem.6c01324
Inorg. Chem. XXXX, XXX, XXX−XXX

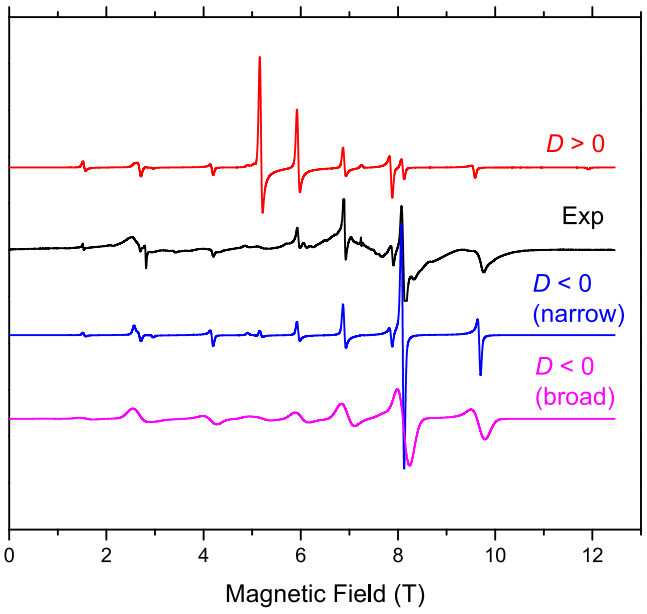

Figure 2. An HFEPR spectrum of $YIn_{0.9}Fe_{0.1}O_3$ recorded at 10 K and 203.2 GHz accompanied by simulations using spin Hamiltonian parameters as obtained from the 2D field vs frequency map through a best fit (see Figure 3). Black trace: experiment; red trace: $D > 0$; blue trace: $D < 0$. A single-crystal line width of 25 mT was used in simulating the narrow resonances, while the broader turning points used a line width of 125 mT. Exactly the same values of the zfs parameters were used in both simulations.

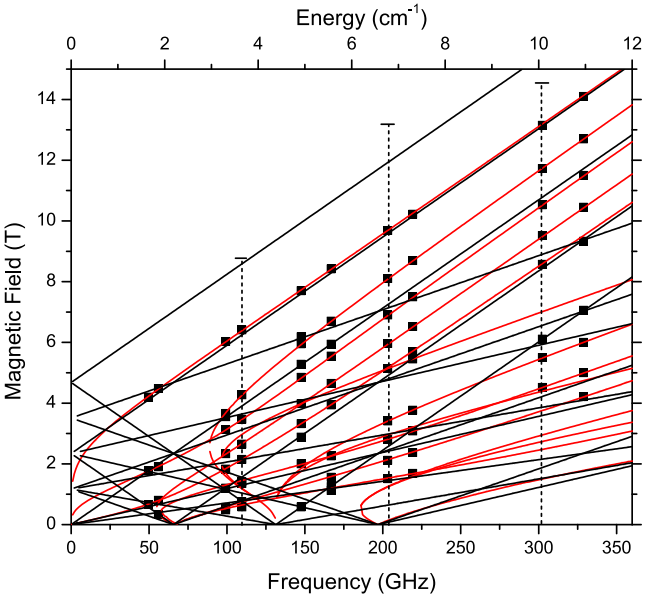

Figure 3. A field vs frequency (or energy) dependence of the turning points in the $YIn_{0.9}Fe_{0.1}O_3$ spectra at 10 K. The squares are experimental resonances, while the curves were simulated using spin Hamiltonian parameters: simulated using the following best-fitted SH parameters: $S = 5/2$, $|D| = 1.095(2)$ cm^{-1}, $|E| = 0.003(4)$ cm^{-1}; $g_\perp = 2.007(1)$, $g_\parallel = 2.004(3)$. Red curves: perpendicular turning points; black curves: parallel turning points. The vertical dashed lines correspond to the frequencies at which spectra presented in Figure S1, Figure 2, and Figure S2, in increasing frequency order, were recorded.

narrow and broad signals. Analogously, a spectrum at $x = 0.1$ and 285 K (Figure 4) still contains both narrow and broad resonances.

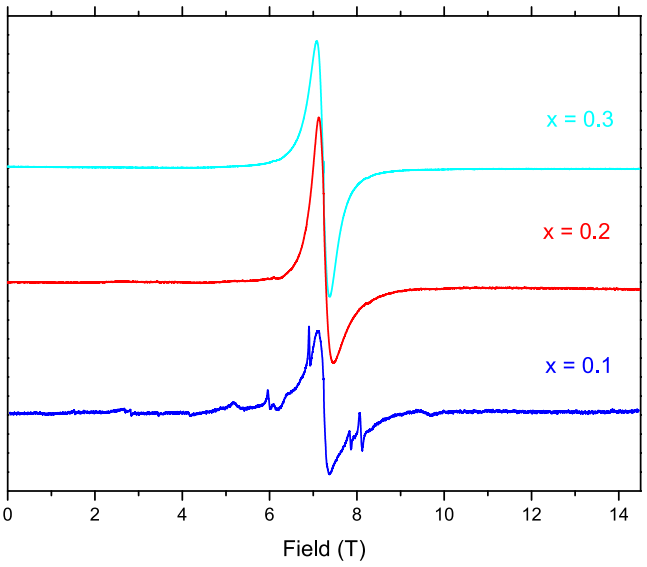

Figure 4. HFEPR spectra of $YIn_{1-x}Fe_xO_3$ with x varying from 0.1 to 0.3, at 203.2 GHz and 280 K.

3.3. Varying Fe^{3+} Concentration with HFEPR Frequency and Temperature Constant

Figure S4 and Figure 4 show EPR spectra recorded at a fixed frequency (203.2 GHz) and temperature (10 and 280 K, respectively), for the Fe^{3+} concentration x varying from 0.1 to 0.3. One can see that the higher the Fe^{3+} concentration, the more pronounced the middle, broad resonance is, at a given temperature. This behavior occurs at any frequency and temperature.

3.4. Varying the Temperature, with HFEPR Frequency and Fe^{3+} Concentration Constant

At any frequency and any doping level of Fe^{3+} from $x = 0.1$ to 0.3, raising the temperature causes the narrow lines visible at low temperature to lose intensity in favor of the broader signals, which in turn merge (coalesce) into one very broad resonance centered on $g = 2.00$ at high enough temperature, as shown in Figure 5 for the case of $x = 0.2$. That resonance in turn undergoes narrowing at yet higher temperatures. This effect is the strongest at the highest concentration of Fe^{3+}, where the narrow resonances observed at low temperature completely disappear under the broad high-temperature signal. For the lowest concentration, $x = 0.1$, some of the narrow lines are still visible, superimposed on the broad high-temperature resonance even at 285 K (Figure S3). A simulation of the set of narrow resonances indicates that the axial zfs parameter $|D|$ undergoes only a modest (ca. −4%) change at 285 K: −1.052 vs −1.095 cm^{-1} at 10 K. Another full temperature dependence, also at 203.2 GHz, is shown for $x = 0.3$ in Figure S5 and is very similar to that observed for $x = 0.2$ except that the narrow resonances disappear at lower temperature in favor of the broad ones.

4. DISCUSSION

4.1. Origin of the Zero-Field Splitting

High-spin d^5 systems such as Fe^{3+}[40] and, more investigated, Mn^{2+},[41−44] generally exhibit small magnitude zfs ($|D| < \sim 1$ cm^{-1}) because their sextet electronic ground state is spherically symmetric as a free ion (^6S) and there are no excited states of the same spin that can couple to the ground state to lead to zfs,

https://doi.org/10.1021/acs.inorgchem.6c01324
Inorg. Chem. XXXX, XXX, XXX−XXX

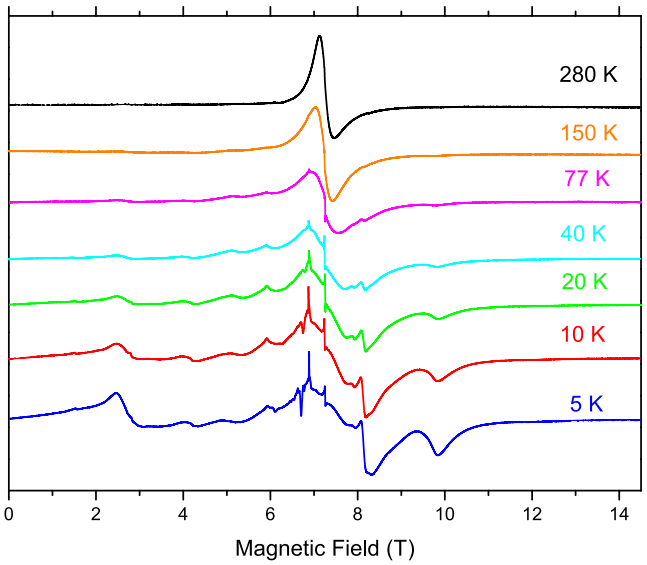

Figure 5. Temperature dependence of the HFEPR spectra of $YIn_{0.8}Fe_{0.2}O_3$ at 203.2 GHz. The spectral position of the single broad resonance emerging with increasing temperature corresponds to g = 2.00.

in contrast to, say, Co^{2+}.[26,45,46] An exception is the strong, axial ligand field present for Fe^{3+} in porphyrin complexes, for which the zfs can be as large as $D \approx 5-20$ cm^{-1},[36,37,47,48] and a satisfying theoretical explanation has yet to be found.[37,38] Biaso et al. provided a comprehensive listing of the zfs parameters of high-spin Fe^{3+} complexes,[32] and selected examples are worth mentioning here. The zfs in high-spin Fe^{3+} as found in frozen aqueous solution $[Fe(EDTA)(H_2O)]^-$ (EDTA = ethylenediaminetetraacetate tetra-anion) is $D = -0.777$ cm^{-1} (−23.3 GHz), $E = -0.21$ cm^{-1} (−6.3 GHz).[31] This species has O and N coordination, so it resembles that of the Fe^{3+} site in $YIn_{1-x}Fe_xO_3$. The crystal structure of $Na[Fe(EDTA)(H_2O)]\cdot 2H_2O$ shows a pentagonal bipyramidal (PBP) geometry about the Fe^{3+} ion,[49] but only roughly so, compared to the truly TBP geometry of Fe^{3+} in $YIn_{1-x}Fe_xO_3$. For Fe^{3+} with homoleptic sulfur coordination, as found in the electron transfer protein rubredoxin (Rd), which has roughly tetrahedral geometry via coordination by four cysteinyl residues, the zfs is larger in magnitude, $D = +1.62(4)$ cm^{-1} (47.5−49.5 GHz), and also very rhombic ($|E/D| = 0.26$). A five-coordinate Fe^{3+} dithiocarbamate ($R_2NCS_2^-$) complex (with $S = 5/2$ ground state), $[Fe(pdtc)_2X]$ (pdtc = pyrrolidine dithiocarbamate; monoanion of pyrrolidine-1-carbodithioic acid), exhibits $D = +2.60$ cm^{-1} for X = Cl and +8.17 cm^{-1} for X = Br.[50] Coordination by heavier (i.e., Period 3 and higher) donors leads to larger magnitude zfs for Fe^{3+}.[36,37] More relevant is Fe^{3+} in aqueous citric acid solutions,[32] where there are only O donors, and the studied complexes are $[Fe(HCit)(H_2Cit)]^{2-}$ at pH 2 and $[Fe(HCit)(Cit)]^{4-}$ at pH 6.2 ($H_4Cit = HOC(CH_2CO_2H)_3$ = citric acid), which respectively exhibit $D = -0.122$ and 0.024 cm^{-1} (sign undetermined; both species with $E \approx 0$). Qualitatively, the zfs of Fe^{3+} in $YIn_{1-x}Fe_xO_3$ is consistent with other such species that have Fe^{3+} with only N,O donors in at least 5-coordination, but with a relatively higher magnitude.

Concerning quantitative aspects of the zfs, its calculation in high-spin d^5 systems is still a challenge, even for those workers who are expert in this area,[37,51,52] which we are decidedly not, particularly for an extended lattice, as opposed to an isolated molecule. We can, however, use a simple ligand-field theory (LFT) model for the isolated TBP $[FeO_{ax2}O_{eq\ 3}]^{7-}$ chromophore as was done in the Mn^{3+} analog.[11] In that system, $d-d$ transitions originating within the ^5D free-ion ground state were clearly assigned that allowed application of LFT in a semiquantitative way. In the present case, however, the electronic transitions are dominated by $Fe^{3+}-O^{2-}$ charge transfer.[2,7] For isolated Fe^{3+} ions, there are no spin-allowed $d-d$ transitions, which precludes such an analysis. The increasing absorption in the Vis region as the Fe concentration increases is due to the development of a band structure,[2,7] which cannot be modeled by simple, single-ion LFT. What can be done is merely to use the bonding parameters determined for Mn^{3+} as an initial estimate for those of Fe^{3+}, which serves well enough for illustration. The structure is shown again in Figure 6, in this case highlighting the TBP Fe^{3+} sites.

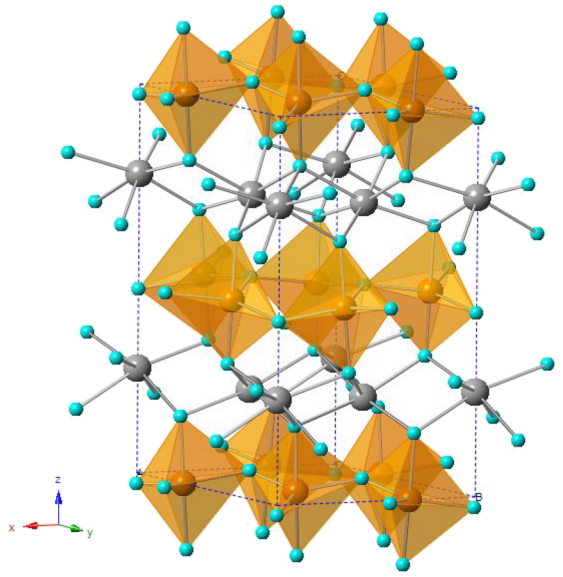

Figure 6. Crystal structure of $YIn_{1-x}Fe_xO_3$ showing MO_5 (M = In, Fe) trigonal bipyramids (TBP) highlighted as orange polyhedra (Y, gray spheres; In/Fe, orange spheres; O, turquoise spheres). The coordinate system is also shown where the z direction corresponds to the TBP axis, as used for the AOM analysis.

To apply LFT, we must assess the structure of the In/Fe site. The bond angles are as follows: equatorial angles, ∠O7−In−O7 = 117.89°, ∠O6−In−O7 = 120.81° (× 2); axial angles: ∠O4−In−O6 = 94.99°, ∠O4−In−O7 = 83.94° (× 2). This is not ideal TBP geometry, but close enough to assume so for our illustrative approach. The axial In/Fe−O distances are 2.078 Å (In−O4) and 2.049 Å (In−O5), while the equatorial distances are 2.101 Å (In−O7 × 2) and 2.103 Å (In−O6)—essentially the same. These metrics indicate that there is axial compression, as discussed in the Mn^{3+} analog. We can then use the angular overlap model (AOM) with a σ-bonding parameter, $\varepsilon_{\sigma eq} = 7000$ cm^{-1}, as a base value for the equatorial ligands and adjust it for the axial ligands using the r^{-5} factor as employed previously $\frac{\varepsilon_{\sigma(Fe-O_{ax})}}{\varepsilon_{\sigma(Fe-O_{eq})}} = \frac{r^5_{(Fe-O_{eq})}}{r^5_{(Fe-O_{ax})}}$. Although there are likely π-interactions between the O donors and the Fe^{3+} ion, we ignore these for the present, simple model. To maintain idealized TBP geometry, which further simplifies the output,

https://doi.org/10.1021/acs.inorgchem.6c01324
Inorg. Chem. XXXX, XXX, XXX−XXX

we use an average axial bond distance, 2.064 Å, which in turn gives a scaling factor of 1.0960, giving $\varepsilon_{\sigma ax}$ = 7670 cm^{-1}. With use of Racah interelectronic repulsion parameters (B and C) that are 85% of the free-ion values,[53] and a spin−orbit coupling (SOC) constant, ζ = 390 cm^{-1} (also 85% of the free-ion value[54]), a zfs with D = −1.44 cm^{-1} results (the ground-state doublet is $m_S = \pm 5/2$). The various parameters (B, C, $\varepsilon_{\sigma ax}$, and ζ) could be independently adjusted to match experiment, as well as reducing the symmetry to C_{3v} by use of different axial bonding parameters (based on the two bond distances). For example, reducing the SOC to ζ = 340 cm^{-1} (∼73% of the free-ion value; still quite reasonable) gives D = −1.088 cm^{-1}, while reducing the bonding parameters to $\varepsilon_{\sigma eq}$ = 6400 cm^{-1} and $\varepsilon_{\sigma ax}$ = 7010 cm^{-1}, giving D = −1.065 cm^{-1}; each calculated value is equivalent to experiment. There is no unique solution within this parameter space, which has not even included varying the Racah parameters. Sample output is given in the Supporting Information, which shows in Table S1 that for $\varepsilon_{\sigma eq}$ = 7000 cm^{-1} and $\varepsilon_{\sigma ax}$ = 7670 cm^{-1}, with absent SOC, the lowest-lying excited state (at ∼10 250 cm^{-1} above the $^6A_1'$ ground state) is a $^4E''$ of 56% ^4G, 35% ^4P free-ion parentage. Thus, considering only the free-ions, there could be SOC between the ^6S ground state and this excited state involving ΔL = +1 and ΔS = −1. The energy of this state is sensitive to the equatorial bonding parameters as it corresponds to an $e''^3e'^2a_1'^0$ MO description (i.e., the ground state of course being $e''^2e'^2a_1'^1$, $d^2_{xz,yz}d^2_{xy,x^2-y^2}d^1_{z^2}$). Thus, considering the individual AOs, the $\hat{l}_y$ and $\hat{l}_x$ operators each respectively connect d_{xz} and d_{yz} with d_{z^2}, again indicating qualitatively how this excited state can lead to zfs via SOC. There is also a doublet excited state, $^2E'$, of very mixed free-ion parentage, at ∼17 240 cm^{-1} above the ground state, which might contribute to zfs via higher-order effects. It can be described roughly as $e''^4e'^1a_1'^0(d^4_{xz,yz}d^1_{xy,x^2-y^2}d^0_{z^2})$. These states including SOC are listed in Table S2 (Supporting Information). Subsequent excited states begin at ∼22 000 cm^{-1} above the ground state (listed only in Table S1), but none has significant (≥10%) ^4P character until a $^4A_2'$ state appears at ∼31 540 cm^{-1} above the ground state. The LFT AOM thus provides at least a simple picture as to the bonding and origin of zfs in this electronically complicated spin sextet Fe^{3+} center.

4.2. Exchange Effects

A striking feature of the HFEPR spectra of $YIn_{1-x}Fe_xO_3$ is the variation of the line width of the turning points depending on two parameters: the doping level of the Fe^{3+} ions, and the temperature (there is little or no dependence on the EPR operation frequency). We attribute these phenomena to exchange effects between the Fe^{3+} located spins, which are extensively covered in the seminal book of Bencini and Gatteschi[55] (reprinted in 2012).[56] Summarizing very briefly the respective chapters (6.1 and 6.2) of that work, in extended lattices such as the currently investigated one, the EPR line width is mainly determined by two major processes: dipolar broadening and exchange narrowing. The resulting value is an interplay of these two phenomena. Keeping this in mind, we may proceed to qualitatively interpret the line widths observed in the $YIn_{1-x}Fe_xO_3$ systems.

While there is apparently little or no dependence of line width on the EPR operating frequency, a striking observation is that at *any* frequency, a spectrum consists of two sets of turning points: one broad, and the other narrow, their line widths differing by an approximate factor of 5 (Figure 2, Figures S1−S3, and Figure 4). Their spectral positions are the same within experimental error, which eliminates a hypothesis that they may originate from different spin species. Rather, a plausible interpretation is that the distribution of the Fe^{3+} ions in the lattice is not completely random, and there exist domains of high concentration that are undergoing strong exchange effects (dipolar broadening) resulting in broad turning points, and domains where the relative concentration of the Fe^{3+} ions is lower, in which the dipolar broadening is much less active. A very similar phenomenon was observed by some of us in the case of V^{2+} ions in solid vanadocene (bis(η5-cyclopentadienyl)vanadium(II))[57] and attributed to an existence of exchanging and nonexchanging domains. There may also be short-range ordering in the In/Fe TBP sites.

While the EPR frequency has little or no effect on the line width, the doping level of Fe^{3+} ions does. The larger the coefficient x, the smaller the participation of the narrow turning points in the spectrum, while the wide features dominate it. At the highest concentration (x = 0.3), the narrow features completely disappear (Figure 5). This is quite straightforward to explain intuitively assuming the domain model outlined above is correct: The higher the Fe^{3+} concentration, the larger the domains of strongly exchanging spins are at the expense of weakly exchanging ones, and hence the dipolar broadening becomes more dominant. At the highest x and at high temperatures, the narrow resonances completely disappear and the exchange narrowing takes over as the line width-limiting mechanism and becomes a global phenomenon; thus, the spectrum is dominated by a single line resulting from averaging the zfs into a single g = 2.00 resonance.

There remains the issue of the temperature dependence of the HFEPR spectra. Of the three parameters affecting the EPR line width in this study, the temperature has the strongest effect and requires careful consideration. Attributing the changes in the EPR line width to exchange effects requires a temperature-dependent exchange mechanism, and we have no proof of that. Alternatively, one could think of the Fe^{3+} ions occupying spaces in the lattice that have somewhat lower energy (on the order of kT) relative to that lattice and being thermally activated at higher temperatures. For that, we have no proof either. What seems plausible instead is the relaxation behavior of the Fe^{3+} spins. Assuming a homogeneous relaxation mechanism, increasing the relaxation rate with temperature leads to line broadening, which could explain the phenomena we see in EPR. However, this is still speculation, and we prefer to leave the matter as is.

5. CONCLUSIONS

The effectiveness of HFEPR in extracting accurate and precise spin Hamiltonian parameters for paramagnetic centers with $S > 1/2$ is again demonstrated in an S = 5/2 Fe^{3+} site with TBP geometry, as is found in $YIn_{1-x}Fe_xO_3$. This material can be prepared in a wide range of doping levels and exhibits a corresponding range of colors from yellow to orange to red brown, making it potentially useful as a pigment. The EPR spectral appearance is highly sensitive to the doping level as well as to temperature. At low temperature and doping (x < 0.3), the material exhibits well-resolved HFEPR spectra that allow the zfs to be determined. Use of LFT with the AOM, as had been done for the blue Mn^{3+} analog, provides a semiquantitative description of the bonding in TBP Fe^{3+} as

https://doi.org/10.1021/acs.inorgchem.6c01324
Inorg. Chem. XXXX, XXX, XXX−XXX

found in $YIn_{1-x}Fe_xO_3$ and provides an estimate of the zfs in good agreement with experiment. A relatively low-lying quartet excited state that corresponds to $d^3_{xz,yz}d^2_{xy,x^2-y^2}d^0_{z^2}$ is likely the primary source of zfs via SOC with the $d^2_{xz,yz}d^2_{xy,x^2-y^2}d^1_{z^2}$ sextet ground state.

■ ASSOCIATED CONTENT

Data Availability Statement

The raw HFEPR files that support the findings of this study are available in the Open Science Framework repository at https://osf.io/xa8mk/.

Supporting Information

The Supporting Information is available free of charge at https://pubs.acs.org/doi/10.1021/acs.inorgchem.6c01324.

HFEPR spectra and LFT output (PDF)

■ AUTHOR INFORMATION

Corresponding Authors

J. Krzystek − *National High Magnetic Field Laboratory, Florida State University, Tallahassee, Florida 32310, United States;* orcid.org/0000-0001-6088-1936; Email: krzystek@magnet.fsu.edu

Mas A. Subramanian − *Department of Chemistry, Oregon State University, Corvallis, Oregon 97331, United States;* orcid.org/0000-0001-5487-043X; Email: Mas.Subramanian@oregonstate.edu

Authors

Joshua Telser − *Department of Biological, Physical and Health Sciences, Roosevelt University, Chicago, Illinois 60605, United States;* orcid.org/0000-0003-3307-2556

Peng Jiang − *Department of Chemistry, Oregon State University, Corvallis, Oregon 97331, United States;* orcid.org/0000-0003-3594-5859

Gopika M. Gopakumar − *Department of Chemistry, Oregon State University, Corvallis, Oregon 97331, United States*

Complete contact information is available at: https://pubs.acs.org/10.1021/acs.inorgchem.6c01324

Notes

The authors declare no competing financial interest.

■ ACKNOWLEDGMENTS

Part of this work was performed at the National High Magnetic Field Laboratory (NHMFL), funded by National Science Foundation through Cooperative Agreements DMR 1157490, 1644779 and 2128556, and the State of Florida. The work done at Oregon State University was supported by NSF Grant No. DMR 2025615 (M.A.S.). We thank Dr. A. Ozarowski (NHMFL) for his EPR simulation and fit program SPIN and Prof. Jesper Bendix (U. of Copenhagen) for Ligfield software.

■ REFERENCES

(1) Smith, A. E.; Mizoguchi, H.; Delaney, K.; Spaldin, N. A.; Sleight, A. W.; Subramanian, M. A. Mn^{3+} in Trigonal Bipyramidal Coordination: A New Blue Chromophore. *J. Am. Chem. Soc.* **2009**, *131*, 17084−17086.

(2) Jiang, P.; Li, J.; Sleight, A. W.; Subramanian, M. A. New Oxides Showing an Intense Orange Color Based on Fe^{3+} in Trigonal-Bipyramidal Coordination. *Inorg. Chem.* **2011**, *50*, 5858−5860.

(3) Smith, A. E.; Sleight, A. W.; Subramanian, M. A. Synthesis and properties of solid solutions of hexagonal $YCu_{0.5}Ti_{0.5}O_3$ with YMO_3 (M = Mn, Cr, Fe, Al, Ga, and In). *Mater. Res. Bull.* **2011**, *46*, 1−5.

(4) Li, J.; Lorger, S.; Stalick, J. K.; Sleight, A. W.; Subramanian, M. A. From Serendipity to Rational Design: Tuning the Blue Trigonal Bipyramidal Mn^{3+} Chromophore to Violet and Purple through Application of Chemical Pressure. *Inorg. Chem.* **2016**, *55*, 9798−9804.

(5) Yamaguchi, O.; Takemura, H.; Yamashita, M.; Hayashida, A. Formation of Yttrium Iron Oxides Derived from Alkoxides. *J. Electrochem. Soc.* **1991**, *138*, 1492−1494.

(6) Li, J.; Singh, U. G.; Schladt, T. D.; Stalick, J. K.; Scott, S. L.; Seshadri, R. Hexagonal $YFe_{1-x}Pd_xO_{3-\delta}$: Nonperovskite Host Compounds for Pd^{2+} and Their Catalytic Activity for CO Oxidation. *Chem. Mater.* **2008**, *20*, 6567−6576.

(7) Li, J.; Subramanian, M. A. Inorganic pigments with transition metal chromophores at trigonal bipyramidal coordination: Y(In,Mn)O_3 blues and beyond. *J. Solid State Chem.* **2019**, *272*, 9−20.

(8) Liu, J.; He, F.; Chen, L.; Qin, X.; Zhao, N.; Huang, Y.; Peng, Y. Novel hexagonal-$YFeO_3$/α-Fe_2O_3 heterojunction composite nanowires with enhanced visible light photocatalytic activity. *Mater. Lett.* **2016**, *165*, 263−266.

(9) Guo, Y.; Zhang, N.; Huang, H.; Li, Z.; Zou, Z. A novel wide-spectrum response hexagonal $YFeO_3$ photoanode for solar water splitting. *RSC Adv.* **2017**, *7*, 18418−18420.

(10) Zhang, R.; Xiong, S.; Gong, M.; Wang, X.; Yu, C.; Lan, J. Influence of substrate orientation on structural, ferroelectric and piezoelectric properties of hexagonal $YFeO_3$ films. *J. Electroceram.* **2018**, *40*, 156−161.

(11) Krzystek, J.; Telser, J.; Li, J.; Subramanian, M. A. Magnetic Properties and Electronic Structure of Manganese-Based Blue Pigments: A High-Frequency and -Field EPR Study. *Inorg. Chem.* **2015**, *54*, 9040−9045.

(12) Krzystek, J.; Telser, J.; Hoffman, B. M.; Brunel, L.-C.; Licoccia, S. High-frequency and field EPR investigation of (8,12-diethyl-2,3,7,13,18-hexamethylcorrolato)manganese(III). *J. Am. Chem. Soc.* **2001**, *123*, 7890−7897.

(13) Krzystek, J.; Telser, J.; Knapp, M. J.; Hendrickson, D. N.; Aromí, G.; Christou, G.; Angerhofer, A.; Brunel, L.-C. High-frequency and -field Electron Paramagnetic Resonance of high-spin manganese(III) in axially symmetric coordination complexes. *Appl. Magn. Reson.* **2001**, *23*, 571−585.

(14) Krzystek, J.; Telser, J. High frequency and field EPR spectroscopy of Mn(III) complexes in frozen solutions. *J. Magn. Reson.* **2003**, *162*, 454−465.

(15) Krzystek, J.; Yeagle, G.; Park, J.-H.; Meisel, M. W.; Britt, R. D.; Brunel, L.-C.; Telser, J. High frequency and field EPR spectroscopy of tris(2,4-pentanedionato)manganese(III): investigation of solid-state versus solution Jahn-Teller effects. *Inorg. Chem.* **2003**, *42*, 4610−4618.

(16) Harvey, J. D.; Ziegler, C. J.; Telser, J.; Ozarowski, A.; Krzystek, J. High-frequency and -field EPR investigation of a manganese(III) N-confused porphyrin complex, [Mn(NCTPP)$(py)_2$]. *Inorg. Chem.* **2005**, *44*, 4451−4453.

(17) Krzystek, J.; Ozarowski, A.; Telser, J. Multi-frequency, high-field EPR as a powerful tool to accurately determine zero-field splitting in high-spin transition metal coordination complexes. *Coord. Chem. Rev.* **2006**, *250*, 2308−2324.

(18) Telser, J.; Krzystek, J.; Ozarowski, A. High-frequency and high-field electron paramagnetic resonance (HFEPR): a new spectroscopic tool for bioinorganic chemistry. *J. Biol. Inorg. Chem.* **2014**, *19*, 297−318.

(19) Pascual-Álvarez, A.; Vallejo, J.; Pardo, E.; Julve, M.; Lloret, F.; Krzystek, J.; Armentano, D.; Wernsdorfer, W.; Cano, J. Field-Induced Slow Magnetic Relaxation in a Mononuclear Manganese(III)−Porphyrin Complex. *Chem. Eur. J.* **2015**, *21*, 17299−17307.

(20) Shova, S.; Vlad, A.; Cazacu, M.; Krzystek, J.; Bucinsky, L.; Breza, M.; Darvasiová, D.; Rapta, P.; Cano, J.; Telser, J.; Arion, V. B. A five-coordinate manganese(III) complex of a salen type ligand with a positive axial anisotropy parameter *D*. *Dalton Trans.* **2017**, *46*, 11817−11829.

(21) Bone, A. N.; Stavretis, S. E.; Krzystek, J.; Liu, Z.; Chen, Q.; Gai, Z.; Wang, X.; Steren, C. A.; Powers, X. B.; Podlesnyak, A. A.; Chen, X.-T.; Telser, J.; Zhou, H.; Xue, Z.-L. Manganese tetraphenylporphyrin bromide and iodide. Studies of structures and magnetic properties. *Polyhedron* **2020**, *184*, No. 114488.
(22) Krzystek, J.; Schnegg, A.; Aliabadi, A.; Holldack, K.; Stoian, S. A.; Ozarowski, A.; Hicks, S. D.; Abu-Omar, M. M.; Thomas, K. E.; Ghosh, A.; Caulfield, K. P.; Tonzetich, Z. J.; Telser, J. Advanced Paramagnetic Resonance Studies on Manganese and Iron Corroles with a Formal d4 Electron Count. *Inorg. Chem.* **2020**, *59*, 1075−1090.
(23) Limburg, J.; Vrettos, J. S.; Crabtree, R. H.; Brudvig, G. W.; de Paula, J. C.; Hassan, A.; Barra, A.-L.; Duboc-Toia, C.; Collomb, M.-N. High-Frequency EPR Study of a New Mononuclear Manganese(III) Complex: $[(terpy)Mn(N_3)_3]$ (terpy = 2,2′:6′,2″-Terpyridine). *Inorg. Chem.* **2001**, *40*, 1698−1703.
(24) Mantel, C.; Hassan, A. K.; Pécaut, J.; Deronzier, A.; Collomb, M.-N.; Duboc-Toia, C. A high-frequency and high-field EPR study of new azide and fluoride mononuclear Mn(III) complexes. *J. Am. Chem. Soc.* **2003**, *125*, 12337−12344.
(25) Krzystek, J.; Swenson, D. C.; Zvyagin, S. A.; Smirnov, D.; Ozarowski, A.; Telser, J. Cobalt(II) "Scorpionate" Complexes as Models for Cobalt-Substituted Zinc Enzymes: Electronic Structure Investigation by High-Frequency and -Field Electron Paramagnetic Resonance Spectroscopy. *J. Am. Chem. Soc.* **2010**, *132*, 5241−5253.
(26) Idešicová, M.; Titiš, J.; Krzystek, J.; Boča, R. Zero-Field Splitting in Pseudotetrahedral Co(II) Complexes: a Magnetic, High-Frequency and -Field EPR, and Computational Study. *Inorg. Chem.* **2013**, *52*, 9409−9417.
(27) Plugis, N. M.; Rudd, N. D.; Krzystek, J.; Swenson, D. C.; Telser, J.; Larrabee, J. A. Cobalt(II) "Scorpionate" complexes as electronic ground state models for cobalt-substituted zinc enzymes: Structure investigation by magnetic circular dichroism. *J. Inorg. Biochem.* **2020**, *203*, No. 110876.
(28) Weisser, J. T.; Nilges, M. J.; Sever, M. J.; Wilker, J. J. EPR Investigation and Spectral Simulations of Iron−Catecholate Complexes and Iron−Peptide Models of Marine Adhesive Cross-Links. *Inorg. Chem.* **2006**, *45*, 7736−7747.
(29) Azarkh, M.; Groenen, E. J. J. Simulation of multi-frequency EPR spectra for a distribution of the zero-field splitting. *J. Magn. Reson.* **2015**, *255*, 106−113.
(30) Mathies, G.; Almeida, R. M.; Gast, P.; Moura, J. J. G.; Groenen, E. J. J. Multifrequency EPR Study of Fe^{3+} and Co^{2+} in the Active Site of Desulforedoxin. *J. Phys. Chem. B* **2012**, *116*, 7122−7128.
(31) Mathies, G.; Blok, H.; Disselhorst, J. A.; Gast, P.; van der Meer, H.; Miedema, D. M.; Almeida, R. M.; Moura, J. J.; Hagen, W. R.; Groenen, E. J. Continuous-wave EPR at 275 GHz: Application to high-spin Fe^{3+} systems. *J. Magn. Reson.* **2011**, *210*, 126−132.
(32) Biaso, F.; Duboc, C.; Barbara, B.; Serratrice, G.; Thomas, F.; Charapoff, D.; Béguin, C. High-Field EPR Study of Frozen Aqueous Solutions of Iron(III) Citrate Complexes. *Eur. J. Inorg. Chem.* **2005**, *2005*, 467−478.
(33) Hassan, A. K.; Pardi, L. A.; Krzystek, J.; Sienkiewicz, A.; Goy, P.; Rohrer, M.; Brunel, L.-C. Ultrawide band multifrequency high-field EMR technique: a methodology for increasing spectroscopic information. *J. Magn. Reson.* **2000**, *142*, 300−312.
(34) Telser, J.; Goldfarb, D.; Stoll, S. EPR Interactions − Zero-Field Splittings. In *EPR Spectroscopy: Fundamentals and Methods*; John Wiley & Sons, Ltd, Chichester, UK, 2017; Vol. *6*, pp 207−233.
(35) Bendix, J. Ligfield. In *Comprehensive Coordination Chemistry II, Vol. 2: Fundamentals: Physical Methods, Theoretical Analysis, and Case Studies*, Lever, A. B. P., Ed. Elsevier: Amsterdam, 2003; Vol. *2*, pp 673−676.
(36) Tin, P.; Stavretis, S. E.; Ozerov, M.; Krzystek, J.; Ponomaryov, A. N.; Zvyagin, S. A.; Wosnitza, J.; Chen, C.-C.; Chen, P. P. Y.; Telser, J.; Xue, Z.-L. Advanced Magnetic Resonance Studies of Tetraphenylporphyrinatoiron(III) Halides. *Appl. Magn. Reson.* **2020**, *51*, 1411−1432.
(37) Stavretis, S. E.; Atanasov, M.; Podlesnyak, A. A.; Hunter, S. C.; Neese, F.; Xue, Z.-L. Magnetic Transitions in Iron Porphyrin Halides by Inelastic Neutron Scattering and Ab Initio Studies of Zero-Field Splittings. *Inorg. Chem.* **2015**, *54*, 9790−9801.
(38) Viciano-Chumillas, M.; Blondin, G.; Clémancey, M.; Krzystek, J.; Ozerov, M.; Armentano, D.; Schnegg, A.; Lohmiller, T.; Telser, J.; Lloret, F.; Cano, J. Single-Ion Magnetic Behaviour in an Iron(III) Porphyrin Complex: A Dichotomy Between High Spin and 5/2−3/2 Spin Admixture. *Chem. Eur. J.* **2020**, *26*, 14242−14251.
(39) Krzystek, J.; Zvyagin, S. A.; Ozarowski, A.; Trofimenko, S.; Telser, J. Tunable-frequency high-field electron paramagnetic resonance. *J. Magn. Reson.* **2006**, *178*, 174−183.
(40) Neese, F.; Solomon, E. I. Calculation of Zero-Field Splittings, g-Values, and the Relativistic Nephelauxetic Effect in Transition Metal Complexes. Application to High-Spin Ferric Complexes. *Inorg. Chem.* **1998**, *37*, 6568−6582.
(41) Duboc, C.; Phoeung, T.; Jouvenot, D.; Blackman, A. G.; McClintock, L. F.; Pécaut, J.; Collomb, M.-N.; Deronzier, A. High-field EPR investigation of a series of mononuclear Mn(II) complexes doped into Zn(II) hosts. *Polyhedron* **2007**, *26*, 5243−5249.
(42) Pichon, C.; Mialane, P.; Rivière, E.; Blain, G.; Dolbecq, A.; Marrot, J.; Sécheresse, F.; Duboc, C. The Highest *D* Value for a Mn^{II} Ion: Investigation of a Manganese(II) Polyoxometalate Complex by High-Field Electron Paramagnetic Resonance. *Inorg. Chem.* **2007**, *46*, 7710−7712.
(43) Duboc, C.; Collomb, M.-N.; Pécaut, J.; Deronzier, A.; Neese, F. Definition of Magneto-Structural Correlations for the Mn^{II} Ion. *Chem. Eur. J.* **2008**, *14*, 6498−6509.
(44) Zein, S.; Duboc, C.; Lubitz, W.; Neese, F. A Systematic Density Functional Study of the Zero-Field Splitting in Mn(II) Coordination Compounds. *Inorg. Chem.* **2008**, *47*, 134−142.
(45) Boča, R. Zero-field splitting in metal complexes. *Coord. Chem. Rev.* **2004**, *248*, 757−815.
(46) Boča, R. Magnetic Parameters and Magnetic Functions in Mononuclear Complexes Beyond the Spin-Hamiltonian Formalism. *Struct. Bonding (Berlin)* **2006**, *117*, 1−264.
(47) Nehrkorn, J.; Martins, B. M.; Holldack, K.; Stoll, S.; Dobbek, H.; Bittl, R.; Schnegg, A. Zero-field splittings in metHb and metMb with aquo and fluoro ligands: a FD-FT THz-EPR study. *Mol. Phys.* **2013**, *111*, 2696−2707.
(48) Hunter, S. C.; Podlesnyak, A. A.; Xue, Z.-L. Magnetic Excitations in Metalloporphyrins by Inelastic Neutron Scattering: Determination of Zero-Field Splittings in Iron, Manganese, and Chromium Complexes. *Inorg. Chem.* **2014**, *53*, 1955−1961.
(49) Solans, X.; Font Altaba, M.; Garcia-Oricain, J. Crystal structures of ethylenediaminetetraacetato metal complexes. V. Structures containing the $[Fe(C_{10}H_{12}N_2O_8)(H_2O)]^-$ anion. *Acta Cryst. C* **1984**, *40*, 635−638.
(50) Brackett, G. C.; Richards, P. L.; Caughey, W. S. Far-infrared magnetic resonance in Fe(III) and Mn(III) porphyrins, myoglobin, hemoglobin, ferrichrome A, and Fe(III) dithiocarbamates. *J. Chem. Phys.* **1971**, *54*, 4383−4401.
(51) Duboc, C. Determination and prediction of the magnetic anisotropy of Mn ions. *Chem. Soc. Rev.* **2016**, *45*, 5834−5847.
(52) Duboc, C.; Collomb, M.-N.; Neese, F. Understanding the Zero-Field Splitting of Mononuclear Manganese(II) Complexes from Combined EPR Spectroscopy and Quantum Chemistry. *Appl. Magn. Reson.* **2010**, *37*, 229−245.
(53) Brorson, M.; Schäffer, C. E. Orthonormal interelectronic repulsion operators in the parametrical d^q model. Application of the model to gaseous ions. *Inorg. Chem.* **1988**, *27*, 2522−2530.
(54) Bendix, J.; Brorson, M.; Schäffer, C. E. Accurate empirical spin orbit coupling parameters z_{nd} for gaseous nd^q transition metal ions. The parametrical multiplet term model. *Inorg. Chem.* **1993**, *32*, 2838−2849.
(55) Bencini, A.; Gatteschi, D. *Electron Paramagnetic Resonance of Exchange Coupled Systems*; Springer Verlag: Berlin, Germany, 1990.
(56) Bencini, A.; Gatteschi, D. *EPR of Exchange Coupled Systems*; Dover Publications, Inc.: Mineola, NY, 2012; p 287.
(57) Jackson, T. A.; Krzystek, J.; Ozarowski, A.; Wijeratne, G. B.; Wicker, B. F.; Mindiola, D. J.; Telser, J. Vanadocene *de Novo*:

https://doi.org/10.1021/acs.inorgchem.6c01324
Inorg. Chem. XXXX, XXX, XXX−XXX

Spectroscopic and Computational Analysis of Bis(η5-cyclopentadienyl)vanadium(II). *Organometallics* **2012**, *31*, 8265−8274.

https://doi.org/10.1021/acs.inorgchem.6c01324
Inorg. Chem. XXXX, XXX, XXX−XXX